Journal of Materials Chemistry C

Green Syntheses of Stable and Efficient Organic Dyes for Organic Hybrid Light-Emitting Diodes

Journal:	*Journal of Materials Chemistry C*
Manuscript ID	TC-ART-04-2021-001567.R1
Article Type:	Paper
Date Submitted by the Author:	30-Apr-2021
Complete List of Authors:	Huang, Yunping; University of Washington, Materials Science & Engineering Cohen, Theodore; University of Washington, Molecular Engineering and Science Institute; University of Washington, Chemistry; University of Washington, Materials Science and Engineering Sommerville, Parker; University of Washington, Chemistry Luscombe, Christine; University of Washington, Materials Science & Engineering

ARTICLE

Green Syntheses of Stable and Efficient Organic Dyes for Organic Hybrid Light-Emitting Diodes

Received 00th January 20xx,
Accepted 00th January 20xx

DOI: 10.1039/x0xx00000x

Yunping Huang,[a] Theodore A. Cohen,[b] Parker J. W. Sommerville [c] and Christine K. Luscombe*[abc]

Organic hybrid light-emitting diodes (hybrid-LEDs) employ organic dyes as light converters on top of commercial blue inorganic LEDs, replacing incumbent inorganic phosphor light converters synthesized from rare-earth and/or toxic metallic elements to optimize device environmental sustainability. Here, we present two naturally derived organic dyes for hybrid-LEDs, highlighting stability and efficiency enhancement based on a novel "acceptor-acceptor" molecular design. This "acceptor-acceptor" skeleton comprises theobromine and thiadiazole, two electron-withdrawing groups that lower energy levels and suppress photooxidation. This differentiates from the widely adopted "donor-acceptor" skeleton, where photooxidation is facilitated by the presence of electron-donating units. Simultaneously, sidechains on organic dyes used to enhance solution processability, crucial for film transparency, introduce an additional photooxidation pathway. With this "acceptor-acceptor" skeleton, the destabilization from sidechains was offset by the stability enhancement from the electronic effects in the backbone. When blended within an industrial polymer, poly(styrene-butadiene-styrene) (SBS), their enhanced solubility enables the formation of highly transparent films, crucial for reducing scattering loss in LEDs. Furthermore, resultant dye-SBS films achieved photoluminescence quantum yields (PLQYs) of around 90% under ambient conditions. Taking advantage of its transparency and solution processability, we fabricated a waveguide with this theobromine-dye-SBS composite, which was subsequentially assembled into an edge-lit LED device of no glare and enhanced aesthetics.

Introduction

LEDs are the foundation of lighting and display products surrounding us. While they have obtained great success in the commercial market, related research and development activities remain highly active aiming to enhance factors such as energy efficiency, stability, and environmental sustainability.[1-3] Currently, commercial LED products comprise of two key components: an indium gallium nitride LED backlight with emission centered at 450 nm to cover the blue region of the visible spectrum, and powder inorganic phosphors on top converting blue light into longer wavelengths (e.g., green and red) to tune the emission of the device (**Fig. 1**). A drawback of inorganic phosphors is that scattering of the emission from the micron-sized phosphor powders leads to substantial backscattering and subsequent absorption of the emission into the LED chip, and reabsorption losses in the phosphor itself, both of which reduce the overall light output of the final LED device.[1, 4, 5] In addition, there are environmental concerns over the use of inorganic phosphors because they are synthesized from rare-earth and/or heavy metallic elements where mining and refinery activity leads to deforestation, loss of biodiversity and air, water and soil pollution.[1, 6-8] Organic dyes possess environmental advantages over inorganic phosphors because they are π-conjugated molecules made from abundant elements (C, H, N, O, etc.) and are potentially bio-sourced.[9] As shown in Fig. 1, by switching inorganic phosphors in LEDs to organic dyes, the resulting hybrid-LEDs could be manufactured with improved environmental sustainability. Moreover, organic

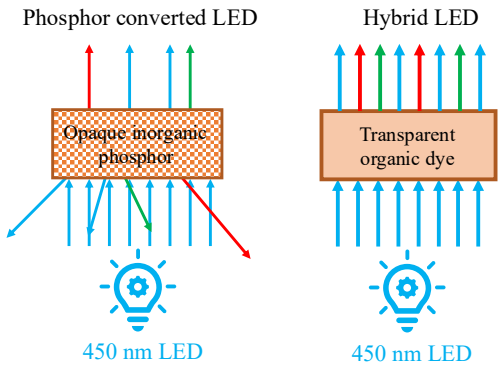

Fig. 1. The structure comparison between a phosphor-converted LED and an organic hybrid-LED. In phosphor converted LEDs, a portion of light is scattered and reabsorbed by the LED chip and phosphor powders, which reduces the overall output of the device.

[a] *Department of Materials Science & Engineering, University of Washington, Seattle, WA 98195, USA.*
[b] *Molecular Engineering & Sciences Institute, University of Washington, Seattle, WA 98195, USA.*
[c] *Department of Chemistry, University of Washington, Seattle, WA 98195, USA.*
Electronic Supplementary Information (ESI) available: [details of any supplementary information available should be included here]. See DOI: 10.1039/x0xx00000x

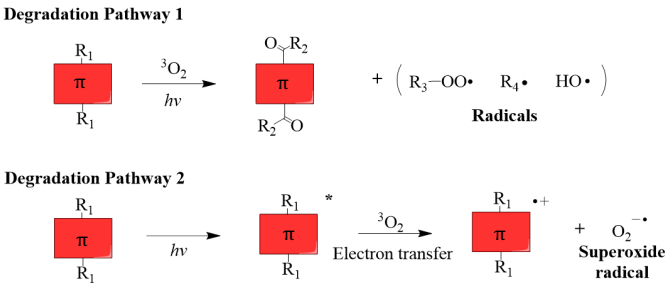

Fig. 2. The mechanisms generating highly reactive radical species responsible for the breakdown of π-conjugated systems. The LUMO alignments and charge transfer mechanism in degradation pathway 2 will be discussed in Section 2.2 and **Fig. 6**.

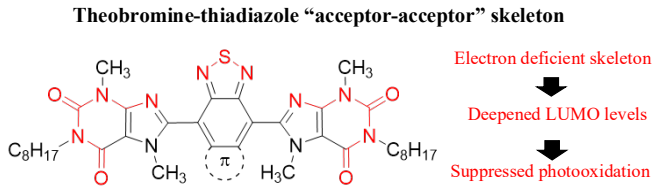

Fig. 3. The structure of the proposed molecular architecture and its structural characteristics to suppress degradation pathway 2.

dyes are fluorescent materials capable of addressing the light scattering problems faced by inorganic phosphors, simply by adjusting solubilizing sidechains attached to their fluorescent cores.[10-12] The appropriate sidechain can hinder the self-aggregation of organic dyes and tune their solution processability, which are crucial for homogeneous materials with high transparency. However, at present most fluorescent dyes are unstable in ambient conditions due to photooxidation,[13-15] a problem which must be addressed before organic hybrid-LEDs become commercially viable.

Fig. 2 summarizes two major degradation pathways of π-conjugated molecules.[13, 14, 16-20] Degradation pathway 1 is directly associated with the sidechains of the π-conjugated molecules. Radicals can form on the methylene groups directly bonded to the π-conjugated backbone or heteroatoms with assistance from oxygen.[19] The resultant radicals can subsequently initiate the degradation of the π-conjugated molecule. Degradation pathway 2 is associated with the reactivity of organic dyes towards ground-state triplet oxygen ($^3O_2$) in the atmosphere. When an organic dye molecule is excited by light, an electron will be promoted to the lowest unoccupied molecular orbital (LUMO) from the highest occupied molecule orbital (HOMO). When the LUMO of the organic dye is shallower than the electron affinity (EA) of $^3O_2$ (-3.75 eV), it is energetically favorable for the electron in the LUMO of the organic dye to transfer to $^3O_2$. This is followed by the formation of a radical cation of the π-conjugated moiety and a superoxide radical ($O_2^{-\bullet}$), the latter of which is highly reactive and initiates the degradation of the π-conjugated structure. Notably, it has been concluded that singlet oxygen ($^1O_2$) has minimal effect on the degradation of the organic semiconductors investigated.[14, 21]

Considering the significance of sidechains for transparent high-performance materials, it is more practical to enhance their stability *via* lowering the energy levels of organic dyes instead of removing sidechains. Introducing electron-withdrawing moieties into organic dye lowers their energy levels.[10, 11] Therefore, in this contribution we present a novel "acceptor-acceptor" skeleton for fluorescent organic dyes with enhanced stability, comprising thiadiazole and theobromine as shown in **Fig. 3**. Thiadiazole is an electron-withdrawing moiety; its derivatives, such as benzo[c][1,2,5]thiadiazole (BT)[22-24] and naphtho[2,3-c][1,2,5]thiadiazole (NT),[25, 26] have been applied in the design of high-performance OLEDs covering wavelengths from green to infrared. Recently, electron-withdrawing theobromine was used in a low-cost and green molecule design that suppresses aggregation caused quenching of fluorescence, which is crucial for synthesizing materials with high photoluminescence quantum yields (PLQYs), while simultaneously enhancing solution processability of organic dyes.[27] Chromophores are covalently linked to alkylated theobromine at the 9 position, sterically repulsing the methyl group at the 8 position of theobromine (Fig.3). The resulting molecules therefore adopt highly twisted conformations with large dihedral angles between the chromophore and the theobromine moiety, which prevents the close interaction among chromophores and therefore suppresses aggregation caused quenching (ACQ) of fluorescence. We hypothesized that by incorporating these two electron-withdrawing moieties in a single molecule, the HOMO and LUMO energy levels would be substantially lowered. This should inhibit degradation pathway 2, an additional benefit along with the previously observed improvements in fluorescence and processability crucial for film transparency. To examine our hypothesis, two molecules consisting of theobromine and thiadiazole, Theo-Green and Theo-Red (Fig. 3), were synthesized respectively. Four other structurally representative organic dyes were included in the experiment to determine the scope of this hypothesis, which affords a comprehensive understanding of the relationship between structure and photostability.

Results and discussion

2.1. The Streamlined Syntheses of Theo-Green and Theo-Red

Theo-Green and Theo-Red were synthesized according to **Scheme 1** using a concise and straight-forward pathway. To begin with, an *n*-octyl chain was attached to theobromine (an abundant non-toxic natural product) to increase the solubility and processability of the final products. Alkylation on theobromine afforded the intermediate in quantitative yield. The second and final step in this simple synthesis is direct arylation, an atom- and step-efficient cross-coupling methodology,[28, 29] to couple the octyltheobromine with chromophores of interest to yield the final products. Compared to Suzuki and Stille coupling commonly applied in organic dye syntheses, direct arylation requires no pre-functionalization to the boronic ester or organotin intermediate. This shortens the overall synthetic procedure and bypasses the use of explosive

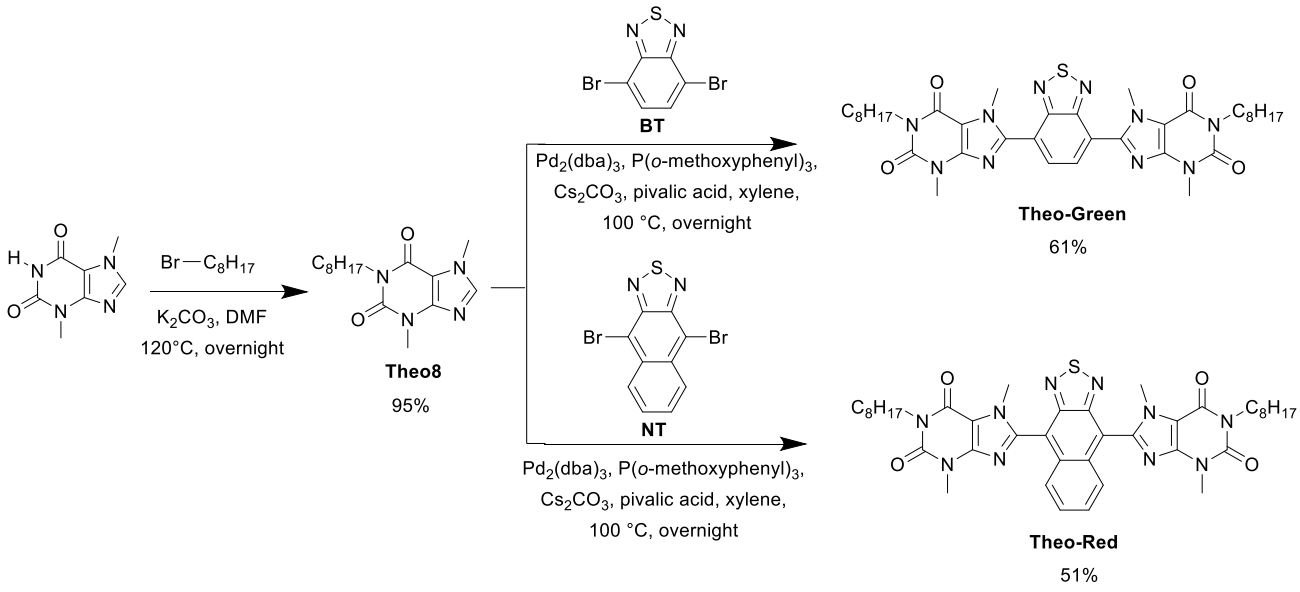

Scheme 1. The synthetic routes of Theo-Green and Theo-Red.

organolithium or toxic organotin compounds, further lowering the cost and environmental risk in industry-scale production.[29] The cross-coupling reaction between octyltheobromine and BT and NT yields the green-emitting Theo-Green and the red-emitting Theo-Red in decent yields, 61% and 51%, respectively.

Fig. 4 shows the absorption and photoluminescence spectra of Theo-Green and Theo-Red with the emission spectra of BT and NT for comparison. The PL of Theo-Green and Theo-Red are red-shifted compared to those of their original chromophores, BT and NT respectively, indicating the theobromine moieties are conjugated to the center chromophores. **Fig. S2.2** shows frontier molecular orbital simulations of Theo-Green and Theo-Red generated based on the B3LYP functional and 6-31g(d) basis set. HOMOs of Theo-Green and Theo-Red extends throughout the whole molecules, while their LUMOs are more localized on the BT/NT core. This indicates a weak charge transfer feature in their HOMO-LUMO transitions while the local excited feature is predominant. The charge transfer feature is more pronounced in Theo-Red as demonstrated by the less spatial overlap between its HOMO and LUMO. This introduction of theobromine extends the conjugation of the BT/NT core and thus led to redshift emissions of Theo-Green and Theo-Red as regards to BT and NT respectively. We observed little overlap between their absorption and emission spectra, which is stemmed from the large dihedral angles between theobromine and the centered chromophores.[27] This minimal overlap between absorption and emission, namely minimal self-absorption, is essential in minimizing light attenuation within materials and increasing the efficiency of final devices, including not only hybrid-LEDs, but also lasers and luminescence solar concentrators. [30, 31]

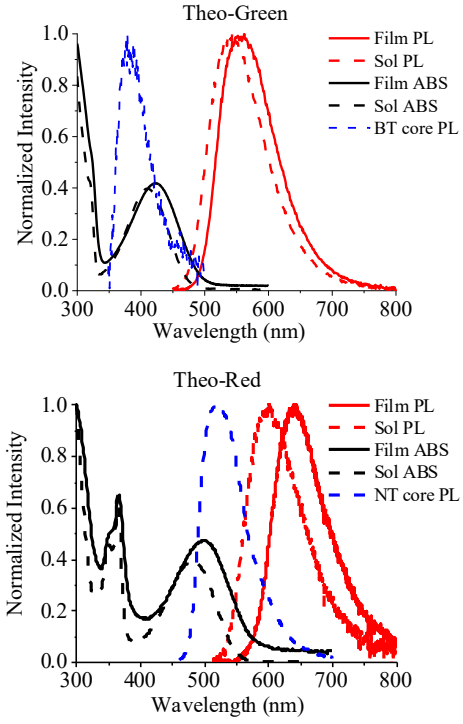

Fig. 4. The absorption (ABS) and photoluminescence (PL) spectra of Theo-Green (left) and Theo-Red (right) in 10^{-5} M chloroform solutions (Sol) and as thin films. The PL of benzo[c][1,2,5]thiadiazole (BT) and naphtho[2,3-c][1,2,5]thiadiazole (NT) in chloroform is also included.

2.2. Structure-Photostability Relationship

Scheme 2 shows other organic dyes we studied to illustrate the relationship between structure and photostability. The selection criteria are as follows: First, BT-TPA and Theo-Green both contain a BT core, but the triphenylamine (TPA) moieties in BT-TPA are electron-donating with no side chains. This is in contrast with the electron-withdrawing alkylated theobromine, allowing direct comparison of the two degradation pathways in Fig. 2. It is worth mentioning that TPA is a popular building block for widely applied "donor-acceptor" dye molecules,[10, 11, 28, 32-35] which is also in contrast to our "acceptor-acceptor" design.

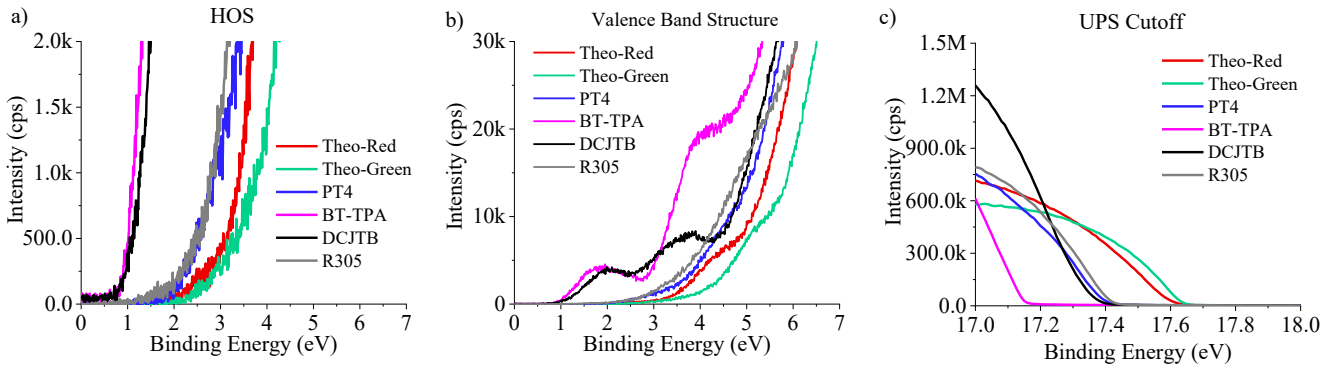

Fig. 5. UPS results of the six organic dyes.

Second, the TPA counterpart for Theo-Red, NT-TPA, absorbs little light around 450 nm and was excluded from this study,[36] as 450 nm is a standard backlight for most LEDs and well absorbed by the other dyes. Third, PT4[27] was chosen to better illustrate the significance of the electron-withdrawing thiadiazole on stability within the theobromine derived molecules. Compared to Theo-Green and Theo-Red, PT4 possesses a shallower LUMO, as pyrene is electron-neutral while BT and NT are both electron-withdrawing. Most commercial organic dyes are not suitable for light converting applications because of fluorescence quenching.[37] However, R305[31] and DCJTB[38-40] are commercial organic dyes that are well-suited for such applications and thus were chosen to expand the scope of the photostability study. While R305 has deep LUMO levels, the LUMO of DCJTB is significantly shallower due to the presence of the electron-donating aryl amine moiety. Therefore it is expected that these two commercial dyes will have distinctly different photostability parameters. *Notably, R305 is one of the most stable fluorescent organic dyes reported thus far,* with its fluorescence intensity unchanged during 6-year of outdoor exposure when imbedded in poly(methyl methacrylate) matrix.[41]

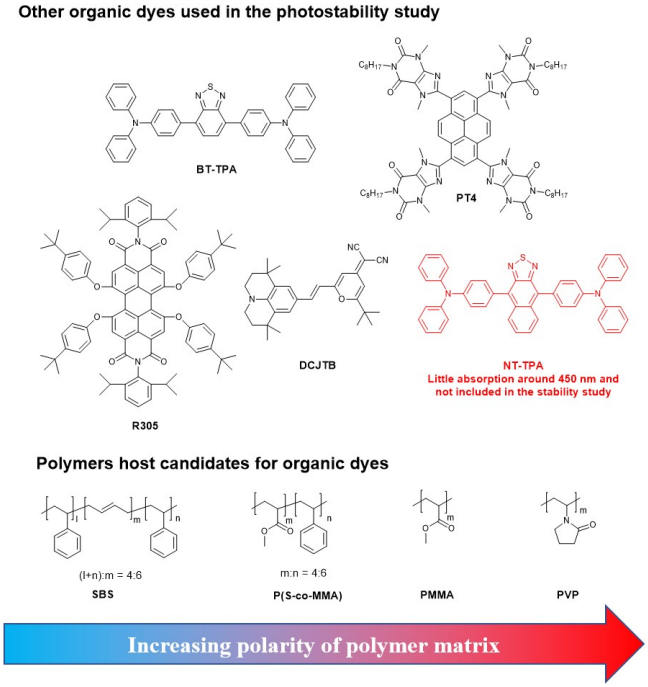

Scheme 2. The structures of other organic dyes studied, and polymers screened for the fabrication of light converting films.

The energy levels of the organic dyes were subsequently determined with UV-Vis absorption spectroscopy and ultraviolet photoelectron spectroscopy (UPS) in tandem. The absolute positions of their HOMOs (E_{HOMO}) were measured by UPS, while their bandgaps (E_g) were calculated from their thin-film absorption onset. The positions of their LUMOs can be estimated with

$$E_{LUMO} = E_{HOMO} + E_g \quad (1)$$

Cyclic voltammetry (CV) was not appropriate for this study because the energy levels of organic dyes shift when in contact with the polar solvents used to prevent dissolution of their thin films during CV measurements.[42]

Fig. 5 shows the UPS He (I) spectra of thin films of Theo-Green, Theo-Red, BT-TPA, PT4, R305 and DCJTB. The energetic position of the top of their HOMOs can be obtained with their highest occupied state (HOS) and cutoffs shown in **Fig. 5a** & **c** with this equation:

$$E_{Top,HOMO} = -(21.2\ eV - (E_{cutoff} - E_{HOS})) \quad (2)$$

Table S1 summarizes these calculations. We noticed that relative to vacuum level, the top of the HOMOs of BT-TPA and DCJTB are -4.94 eV and -4.85 eV respectively, which is distinctly shallower than that of the other compounds. This can be ascribed to their extra valence bands centered at low binding energies as shown in **Fig. 5b**, 1.75 eV and 2.00 eV for BT-TPA and DCJTB respectively, corresponding to -5.77 eV (BT-TPA) and -5.82 eV (DCJTB) relative to vacuum level. Considering that the lone pair electrons of trialkylamines have oxidation potential onsets around -5.1 eV (determined by CV),[43] the formation of these shallow band in BT-TPA and DCJTB can be attributed to the tertiary amines in their conjugated systems. The relatively deeper band position of BT-TPA compared to DCJTB can be ascribed to the additional two adjacent phenyls that lower the electron density of the lone pair on the N atom *via* n-π interaction in BT-TPA. Although there are tertiary amines present in the other organic molecules, their lone pair electrons

are closely interacting with electron-withdrawing groups (carbonyl and imine), which leads to the formation of 3-center 4-electron (3c–4e) π bond and the loss of their lone pair features.[44, 45] Therefore the other compounds do not have these extra bands at lower binding energies.

The position of the bottom of their LUMOs can be calculated with

$$E_{Bottom,LUMO} = E_{Top,HOMO} + E_g \quad (3)$$

and the bandgaps of these six compounds are estimated by UV-vis absorption of their thin films according to

$$E_g = \frac{1240}{\lambda_{cutoff}} \text{ eV} \quad (4)$$

(UV-vis absorptions in **Fig. S3**). Their LUMO positions are summarized in **Table S1** and their frontier band structures are visualized in **Fig. 6**. Two LUMO position trends can be observed in this data: 1) molecules that have uplifted HOMOs, BT-TPA and DCJTB, also possess shallow LUMO levels. 2) For molecules with similar HOMO positions (e.g., PT4, Theo-Red and R305) their LUMO positions deepen as their bandgaps decrease.

Photostability measurements were performed to investigate the structure-photostability relationship. The organic dyes were spin coated into thin films in ambient condition. Photostability measurements of these samples were performed at room temperature in ambient condition under constant, full-area excitation by a 450 nm blue LED (the same wavelength as one of the hybrid LED device) while the PL intensity emanating from the edge of the samples was monitored over time (**Fig. S5.1**). A strong light intensity of ~90 mW/cm² was applied in this experiment to accelerate the degradation experiments. **Fig. 7** shows the evolution of integrated PL intensity of the six molecules as a function of irradiation time. The PL signals of these neat film samples rapidly decrease at the beginning of the stability tests and the rate of degradation decreases with time. We speculated that the fast decay is attributed to the degradation of molecules near the solid-air interface, while the slow decay is attributed to the degradation of the molecules farther away from the solid-air interface, where their degradation is limited by the diffusion of molecular oxygen. This was supported by our degradation experiment of thicker dye-SBS composites, where the fast decay rate changed little compared to the neat films, while the slow decay rate was decreased (see **Fig. S5.2**). Fig. S5.2 shows the degradation profiles of these organic dyes in other polymer matrices. We observed the oxygen permeability and the polarity of the polymer hosts have significant impacts on the photostability of organic dyes and such discussions on extrinsic factors are available in Section 5 in the supporting information.

PT4, BT2, NT2 and R305 have similar structural features (amide groups and alkyl side chains) but different LUMO levels. We observed that R305 has the best stability, followed by NT2, BT2, and PT4, which is consistent with the trend of LUMO depth and increased stability suggested by degradation pathway 2 in Fig. 2. On the other hand, BT-TPA shows significantly higher stability relative to DCJTB and PT4 despite the fact that DCJTB, BT-TPA and PT4 have similar LUMO depths around -3 eV. This

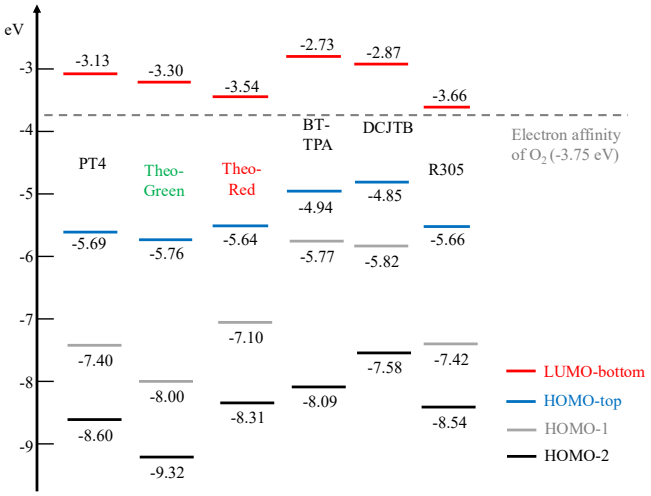

Fig. 6 Frontier band structures of the six organic dyes of interest.

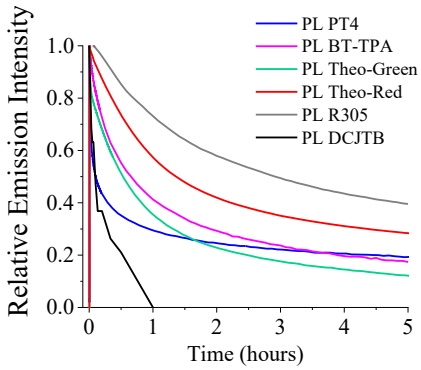

Fig. 7. PL decays of the organic dyes under 450 nm radiation in air. The PL of DCJTB was measured ex situ with an integrating sphere because of aggregation caused quenching and thus low fluorescence as thin film. The setup for stability measurement of the other five dyes are shown in Fig. S5.1.

agrees with degradation pathway 1, where the presence of sidechains accelerates the photodegradation of organic dyes. On the contrary, the stability of Theo-Green is comparable to the stability of BT-TPA, even though the six extra side chains per molecule should significantly facilitate degradation pathway 1. This indicates that degradation pathway 2 in Theo-Green is successfully suppressed by modifying the electron-withdrawing theobromine to lower the LUMO energy level. Notably, the degradation mechanism from singlet oxygen formation could be excluded because we did not observe the formation of singlet oxygen from these six molecules under 450 nm radiation, as shown in **Fig. S6**, which is consistent with previous work.[14, 21] This trend that we observed with these six *fluorescent* dyes agreed with the trend of *non-fluorescent* organic semiconductors used in organic solar cells, together providing a more comprehensive understanding of the degradation of organic semiconductors. [13, 14, 16-20]

Moreover, the above results highlight the importance of the "acceptor-acceptor" design on stability: First, only utilizing one type of acceptor (e.g., PT4) is not sufficient to lower the energy levels enough to decelerate degradation pathway 2, and second, the incorporation of donor moieties is detrimental to stability due to the simultaneous uplifting of HOMO and LUMO (e.g., DCJTB and BT-TPA), which points out the stability

drawback of the commonly applied "donor-acceptor" molecule design. While the stability of Theo-Red is significantly improved compared to most dyes, it did not exceed the current stability record of R305. However, Theo-Red substantially outperforms R305 in hybrid-LEDs due to enhanced fluorescence intensity and transparency, which will be elaborated in the following section.

2.3. Lighting-converting efficacy in hybrid-LEDs

In light of the enhanced stability of the Theo-Green and Theo-Red, we believe these dyes have great commercial potential in hybrid-LEDs. Moreover, Fig. 4 shows that Theo-Green and Theo-Red have large emission bandwidths with full-width half maximums around 100 nm, which is beneficial to obtain lighting devices with high color fidelity index (CFI). CFI is an updated and comprehensive standard proposed recently to address the disadvantages of the incumbent color rendering index (CRI) standard. [46] Recent results have demonstrated it requires a smaller number of large-bandwidth emitters[47] to achieve high CFIs compared to narrow-bandwidth emitters.[48] As shown in Fig. 1, there are two major components in a hybrid-LED: a blue light source and a light-converting layer. In operation, a portion of the blue light emitted from the light source is converted to longer wavelengths by the light converter chosen. As such, the emission of a hybrid-LED is easily tuned by varying the converter, instead of integrating extra LEDs of different colors. The overall efficiency of a hybrid-LED is directly related to the efficiency of the blue LED that converts electricity to blue lights and the efficiency of the light converter that converts blue light into other wavelengths.[1, 3]

PLQYs were used to quantify the light converting efficiency of the organic dyes, which can be directly measured by an integrating sphere. Due to the influence of the bandgap law,[49, 50] it is challenging to obtain narrow bandgap materials, especially red emitters, with high PLQYs. A narrowed bandgap increases the chance of overlapping of vibronic modes between ground states and excited states within an emitter, which facilitates non-radiative decays via electron-phonon coupling and leads to a reduced PLQY. The PLQYs of spin-coated films of Theo-Green and Theo-Red were 46.4% and 30.2% respectively, even with the presence of the theobromine moieties that suppress aggregation quenching. Therefore, external factors are needed to further increase the PLQYs of these dyes and thus the overall efficiency of a final hybrid-LED.

The polarity of the organic dyes' surrounding environments strongly influences their PLQYs – generally PLQYs decrease with increasing polarity. [22, 36] Therefore, the PLQYs of Theo-Green and Theo-Red in solvents of different polarity were measured and summarized in **Table 1**. The PLQYs of both Theo-Green and Theo-Red decrease as the polarity of the solvents increases, which is consistent with the general trend. High polarity environments intramolecular charge transfer states of the excited molecules, where non-radiative decay is more pronounced due to the limited spatial overlap between their HOMOs and LUMOs.[24]

This polarity-PLQY relationship is also applicable in dye-polymer composites. We blended Theo-Green and Theo-Red with different polymers (listed in Scheme 2) at 1 wt% and measured the PLQYs (Table 2). It is observed that the PLQY of the dye-polymer composites decrease as the polarity of the polymers increase. In both solution and thin films, the PLQY of Theo-Red has a stronger dependence on polarity than Theo-Green, which can be explained by the stronger charge transfer feature in its excited state (Fig. S2.2) and the fact that increased polarity of the environment induces larger special separation between its HOMO and LUMO. A slight decrease in PLQYs were observed with increasing content of Theo-Green or Theo-Red in SBS. This PLQY decrease in higher organic dye concentration is associated with an increase of film polarity, considering the polar nature of theobromine. The higher PLQY of the 20:100 Theo-Red-SBS sample compared to 20:100 Theo-Green-SBS can be ascribed to its limited solubility in SBS and aggregation at such a high concentration (Fig. S7). SBS yields the highest PLQYs due to its low polarity and thus was chosen for the subsequent fabrication of the hybrid-LED device.

Table 1. The PLQYs of Theo-Green and Theo-Red solution at the concentration of 10^{-5} M measured with an integrating sphere.

Solvent	Polarity Relative to water	Theo-Green [%]	Theo-Red [%]
Hexane	0.009	96.7	91.3
Toluene	0.099	90.9	77.4
Ether	0.117	92.0	63.2
Anisole	0.198	80.5	43.0
Chloroform	0.259	77.5	45.1
Dichloromethane	0.309	71.8	62.6
Acetonitrile	0.460	2.4	0

Table 2. The PLQYs of Theo-Green and Theo-Red polymer complex with varied blending ratio measured with an integrating sphere. The PLQYs of other four dyes are in **Table S2**.

Polymer host	Film composition Dye:polymer weight ratio	Theo-Green [%]	Theo-Red [%]
SBS	0.1:100	95	90
SBS	1:100	94	87
SBS	10:100	71	61
SBS	20:100	49	56
P(S-co-MMA)	1:100	93	79
PMMA	1:100	91	75
PVP	1:100	80	61

In down-conversion LEDs, PLQYs are also commonly applied in evaluating the light converting efficiency of transparent materials (e.g., organic dyes,[51-53] quantum dots,[54-56] and fluorescent proteins[57-59]). On the other hand, micron-size inorganic phosphors utilize slightly different efficiency metrics compared to the other transparent light converters due to their optically opaque nature; these metrics are external quantum efficiency (EQE) and internal quantum efficiency (IQE). Similar to PLQY, IQE evaluates the non-radiative loss in light conversion. However due to the significant scattering loss within the phosphor powder, it is more accurate to use EQE to describe the down-conversion process of the actual device, leveraging energy loss from both non-radiative decay and scattering.

The scattering loss in transparent composites such as organic dyes and quantum dots are minimal and therefore two parameters are not typically reported and most only report PLQY. As shown in **Table S2**, the PLQYs of Theo-Green and Theo-Red-SBS composites are comparable to the state-of-art results in recent years.

Even though the blending ratio of Theo-Green and Theo-Red must be kept around 1 wt% to maintain high PLQYs around 90%, the low blending ratio is sufficient for hybrid-LED applications. **Fig. 8** shows SBS blends of the Theo-Green, Theo-Red, other organic dyes and a commercial inorganic phosphor with and without UV irradiation. The dye-SBS samples appear to generate sufficient photoluminescence intensity for hybrid-LEDs when the dye:SBS ratios were a scant 1:100. However, the micron-sized inorganic phosphor SGA isophor® from Sigma Aldrich required ~100 times more material to achieve comparable output intensity. This can be ascribed to the fact that micron-size inorganic phosphors are unable to form a homogeneous film and excitation light can easily leak through between particles. This highlights the advantage of the organic dyes in light converting applications regarding material consumption, which helps further lower the cost of final hybrid-LED products in a significant way.

The SBS blends of Theo-Green, Theo-Red and BT-TPA appear to have minimal scattering under low blending ratios. However, only the Theo-Green maintained transparency at a high dye:SBS ratio of 20:100; Theo-Red and BT-TPA appear hazy at a blend ratio 10:100. Transmittance measurements were used to quantify the transparency of these samples (Fig. 8). To eliminate the interference from absorption of the organic dyes, we use the wavelength range from 650 – 700 nm to evaluate the transmission of the different light converting films. Shorter wavelengths (e.g., wavelengths from 450 - 650 nm commonly used in lightings) are more subjective scattering considering scattering intensity is strongly wavelength-dependent ($\sim\lambda^{-4}$), and thus the film transmittance from 650 - 700 nm provides a fair evaluation for light-converting materials in lighting. In the transmittance results, we find that only Theo-Green maintains high transmittance at high blending ratios, around 95% for the 10:100 blend and around 90% for the 20:100 samples. As for Theo-Red and BT-TPA, while the transmittance values of 1:100 blends are around 100%, they drop below 20% when the blending ratio is increased to 20:100. This reduced transparency of BT-TPA and Theo-Red can be ascribed to micron-size particles

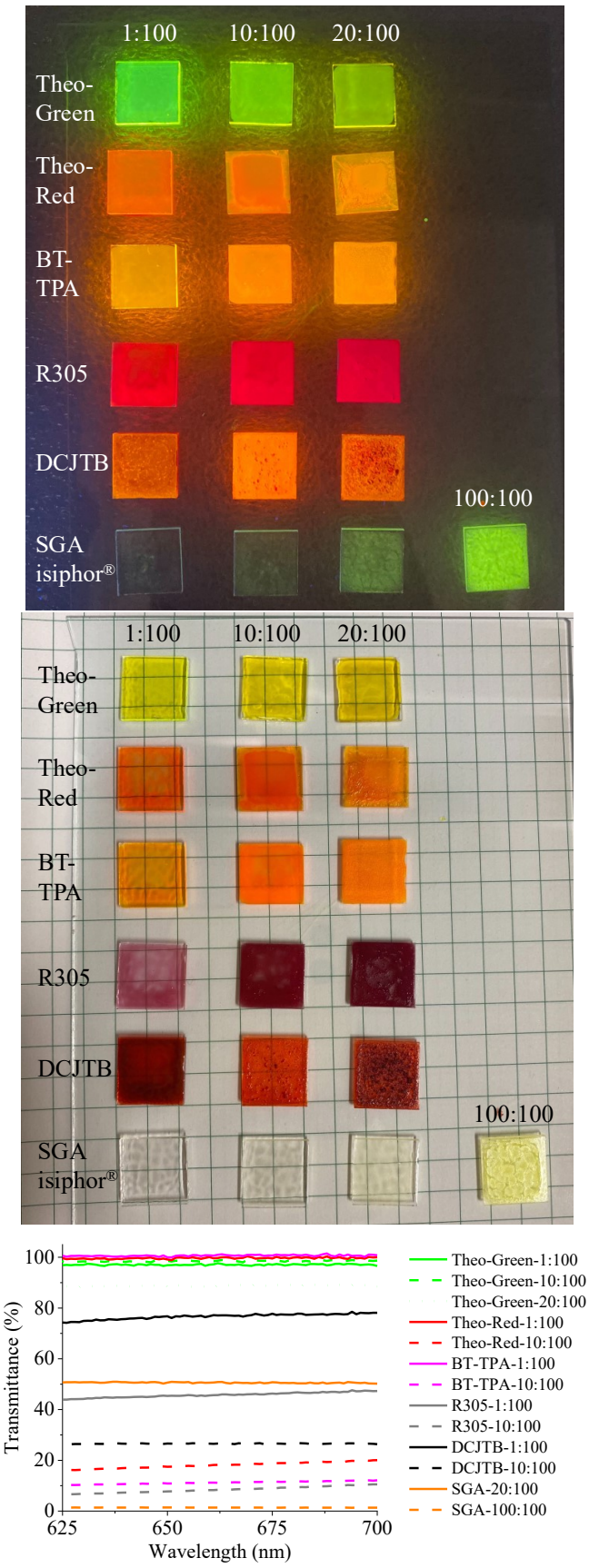

Fig. 8. Comparison of light converting efficacy (top) and transparency (middle) of inorganic phosphors and organic dyes. Blending ratio (converter:SBS) are also labelled. (bottom) transmittance of the light-converting films.

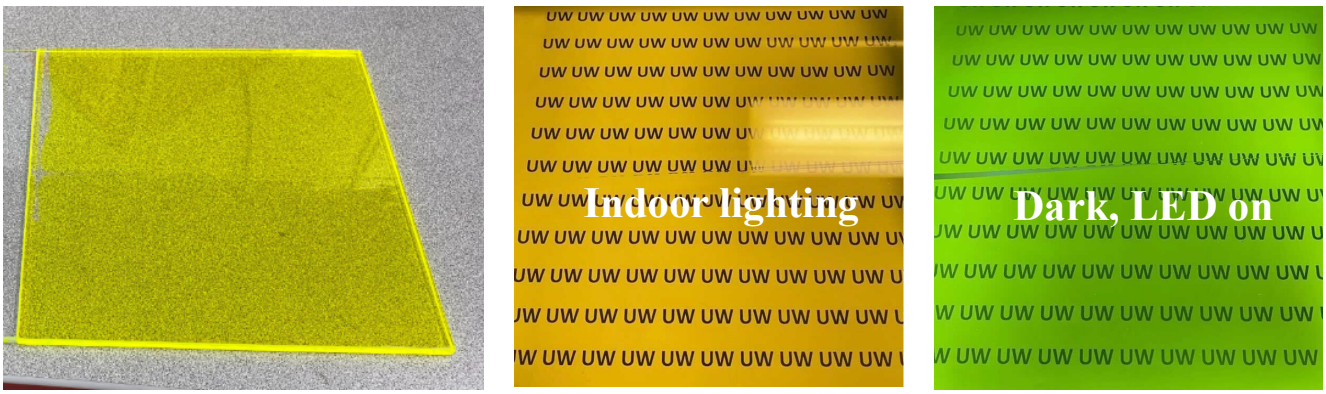

Fig. 9. (left) as-fabricated waveguide by blade-coating the Theo-Green-SBS composite on a glass substrate; (middle & right) demonstration of transparency and non-glare feature of the edge-lit lighting device based on the waveguide shown on the left.

formed in the dye-SBS composites at high blending ratios, while the film of Theo-Green-SBS remained homogeneous (**Fig. S7**). The role of the sidechains in solution processed organic dyes is underlined by these results. Theo-Green and BT-TPA have the same central aromatic unit (BT). Therefore, the difference in transparency must stem from their modifiers – alkylated theobromine endows higher transparency than non-alkylated TPA moieties. Compared with Theo-Green, there is a decrease in transparency in the Theo-Red samples. This is because the larger central aromatic unit (NT) enhances π -π interactions, facilitating the formation of large aggregates. This can be inhibited by changing its octyl sidechain to a longer or branched side chain,[10, 11] which would increase its solubility in the SBS matrix and recover the transparency of the dye-SBS composite. The SBS blends of R305 and DCJTB have limited film transparency due to the formation of micron-size aggregates (Fig. S7) even at a low blending ratio of 1:100. Their film transparency values are below 80% at low blending ratio of 1:100 due to the presence of small aggregates, and their transparency continues to decrease as the blending ratio increases. This is explained by the fact that these two molecules have planar π conjugated structures, and their intermolecular π - π interactions facilitate the formation of large aggregates that scatter light.[37] This is consistent with the results observed by Kim *et al.* utilizing perylene dyes for micro-LED displays.[60] These traditional organic dyes suffer from aggregation when dispersed in a polymer matrix, which leads to opaqueness and fluorescence quenching even at low concentrations, and thus in their experiment the optimal dye mixing ratio was merely 0.6 wt% and the PLQYs were around 40%. However, this is overcome with our molecular design – we were able to enhance the blending ratio to 10 wt% with PLQY of 70% (Theo-Green), providing approximately 30 times increase in optical output. This emphasizes the advantages of introducing alkylated theobromine in the dye structure – preventing aggregation quenching and increasing solubility in the polymer matrix. Based on this result, the conclusion by Kim *et al.* stating "the overall intensity and color-conversion efficiency of organic dyes are low for down-conversion LEDs" should be reconsidered. SGA isophor®-SBS composite also has low transparency. For both organic dyes and inorganic phosphors, low film transparency is disadvantageous in hybrid-LEDs because it leads to scattering losses, which decrease the overall light output of hybrid-LEDs.[4, 5] Notably, because the sizes of traditional inorganic phosphors are usually several microns, the scattering losses in these phosphor-based devices are the most pronounced.[4]

Considering the high transparency of Theo-Green-SBS composite at high dye concentration and its high PLQYs, we subsequently processed it into a waveguide for a non-glare transparent edge-lit device.[61] The dye-imbedded waveguide was fabricated by blade-coating the Theo-Green-SBS (10 wt%) solution onto a 30 cm × 30 cm glass substrate (see the experiment details on Section 9 of supporting information). The edge-lit device was assembled by coupling inorganic LEDs to the edges of the waveguide. As shown in **Fig. 9**, the resulting device overcomes the problematic glares featured in traditional LED lightings, and its transparent appearance comparable to commercial OLED products. The emission spectrum of the device is shown in **Fig S9.2**, showing the sharp emission peak of a blue LED centered at 450 nm and board emission peak from Theo-Green at longer wavelengths. The CIE of the device is (0.3936, 0.5082). We were not able to measure the efficiency of this edge-lit device due to its relatively larger size and dual-side emitting configuration.

Conclusions

In this paper, we used direct arylation and an abundant non-toxic natural product to synthesize two organic dyes (Theo-Green and Theo-Red) for hybrid-LED application, uniting the advantages of inorganic LEDs and OLEDs. These two dyes are comprised of an "acceptor-acceptor" skeleton featuring theobromine and thiadiazole. It was demonstrated that this "acceptor-acceptor" skeleton significantly lowers the energy levels of resultant organic dyes relative to the electron affinity of triplet oxygen to decelerate photooxidation. While the "donor-acceptor" skeleton is sufficient in tuning the bandgap of organic dyes,[11] it facilitates photooxidation due to the presence of electron-donating units, such as arylamines, increasing the energy levels relative to the electron affinity of triplet oxygen. In addition to enhanced stability, the "acceptor-acceptor" design results in organic dyes with high PLQY and enables processability optimization through simply sidechain

modification. We fabricated highly transparent films when Theo-Green and Theo-Red were blended with SBS, which is crucial to reduce light scattering loss in hybrid-LEDs. In addition, these dye-SBS films achieved PLQYs of around 90% under ambient conditions. Such PLQYs are comparable to the state-of-art results from organic dyes, bio-derived phosphors, traditional inorganic phosphors, and quantum dots achieved in recent years. Taking advantage of the enhanced transparency and PLQY of Theo-Green-SBS composite, we were able to fabricate an edge-lit device utilizing waveguide optics and low-cost inorganic LEDs. The resulting device demonstrated enhanced aesthetics comparable to commercial OLED lightings. Considering the aforementioned enhancements on stability, transparency, PLQY, and aesthetics, these theobromine dyes demonstrate potential in high-performance, environmentally sustainable hybrid-LEDs.

Author Contributions

Y.H. and C.K.L. conceived of the presented idea. Y.H. carried out material syntheses and material characterization and took a lead in writing the manuscript. T.A.C carried out material characterization. P.J.W.S. carried out density functional theory calculation. C.K.L. supervised the project. All authors provided critical feedback and helped shape the research, analysis and manuscript.

Conflicts of interest

There are no conflicts to declare.

Acknowledgements

The authors would also like to acknowledge the financial support from the Clean Energy Institute, NSF Partner for Innovation Award (2043422) (Y.H.), NSF Center for Selective C–H Functionalization (CHE-1700982) (C.K.L.), and a Materials Research Science and Engineering Center (DMR-1719797) (T.A.C.). Work by P.J.S.W. was supported by the U.S. Department of Energy (DOE), Office of Science, Basic Energy Sciences (BES) under Award #DE-SC0020046. Y.H. thanks the Data Intensive Research Enabling Clean Technology (DIRECT) NSF National Research Traineeship (DGE-1633216) for support. Y.H. thanks Prof. Daniel R. Gamelin for support with stability measurements. The UPS measurement was conducted by Dr. Samantha Young at the Molecular Analysis Facility, a National Nanotechnology Coordinated Infrastructure (NNCI) site at the University of Washington, which is supported in part by funds from the National Science Foundation (awards NNCI-2025489, NNCI-1542101), the Molecular Engineering & Sciences Institute, and the Clean Energy Institute. The blade-coated waveguide fabrication is conducted in Washington Clean Energy Testbed with help from Dr. Phillip Cox. We would like to thank and acknowledge the staff at the School of Pharmacy's Mass Spectrometry Center at the University of Washington for their instrumentation.

Notes and references

1. P. M. Pattison, M. Hansen and J. Y. Tsao, *C R Phys*, 2018, **19**, 134.
2. D. Chen, W. Xiang, X. Liang, J. Zhong, H. Yu, M. Ding, H. Lu and Z. Ji, *J. Eur. Ceram. Soc*, 2015, **35**, 859.
3. S. Ye, F. Xiao, Y. X. Pan, Y. Y. Ma and Q. Y. Zhang, *Mater. Sci. Eng.,* 2010, **71**, 1.
4. H. K. Park, J. H. Oh and Y. R. Do, *Opt. Express*, 2012, **20**, 10218.
5. M. Nyman, L. E. Shea-Rohwer, J. E. Martin and P. Provencio, *Chem. Mater.*, 2009, **21**, 1536.
6. I. Razo, L. Carrizales, J. Castro, F. Díaz-Barriga and M. Monroy, *Water, Air, and Soil Pollution.*, 2004, **152**, 129.
7. J. J. Swenson, C. E. Carter, J.-C. Domec and C. I. Delgado, *PLOS ONE*, 2011, **6**, 18875.
8. L. J. Sonter, S. H. Ali and J. E. M. Watson, *Proc. Biol. Sci.*, 2018, **285**, 20181926.
9. V. R. Feig, H. Tran and Z. Bao, *ACS Cent. Sci.*, 2018, **4**, 337.
10. Y. Huang, D. L. Elder, A. L. Kwiram, S. A. Jenekhe, A. K. Y. Jen, L. R. Dalton and C. K. Luscombe, *Adv. Mater.*, 2019, 1904239.
11. Y.-J. Cheng, S.-H. Yang and C.-S. Hsu, *Chem. Rev.*, 2009, **109**, 5868.
12. A. C. Grimsdale, K. L. Chan, R. E. Martin, P. G. Jokisz and A. B. Holmes, *Chem. Rev.*, 2009, **109**, 897.
13. E. M. Speller, A. J. Clarke, J. Luke, H. K. H. Lee, J. R. Durrant, N. Li, T. Wang, H. C. Wong, J.-S. Kim, W. C. Tsoi and Z. Li, *J. Mater. Chem. A*, 2019, **7**, 23361.
14. M. Jørgensen, K. Norrman, S. A. Gevorgyan, T. Tromholt, B. Andreasen and F. C. Krebs, *Adv. Mater.*, 2012, **24**, 580.
15. C. Zhao and L. Duan, *J. Mater. Chem. C*, 2020, **8**, 803.
16. M. Manceau, A. Rivaton, J.-L. Gardette, S. Guillerez and N. Lemaître, *Polym. Degrad. Stab.*, 2009, **94**, 898.
17. M. Manceau, J. Gaume, A. Rivaton, J.-L. Gardette, G. Monier and L. Bideux, *Thin Solid Films*, 2010, **518**, 7113.
18. A. Rivaton, S. Chambon, M. Manceau, J.-L. Gardette, N. Lemaître and S. Guillerez, *P Polym. Degrad. Stab.*, 2010, **95**, 278.
19. A. Rivaton, A. Tournebize, J. Gaume, P.-O. Bussière, J.-L. Gardette and S. Therias, *Polym. Int.,* 2014, **63**, 1335.
20. E. M. Speller, A. J. Clarke, N. Aristidou, M. F. Wyatt, L. Francàs, G. Fish, H. Cha, H. K. H. Lee, J. Luke, A. Wadsworth, A. D. Evans, I. McCulloch, J.-S. Kim, S. A. Haque, J. R. Durrant, S. D. Dimitrov, W. C. Tsoi and Z. Li, *ACS Energy Lett.*, 2019, **4**, 846.
21. M. Manceau, A. Rivaton and J.-L. Gardette, *Macromol. Rapid Commun.*, 2008, **29**, 1823.
22. L. Yao, S. Zhang, R. Wang, W. Li, F. Shen, B. Yang and Y. Ma, *Angew. Chem. Int. Ed.*, 2014, **53**, 2119.
23. Will W. H. Lee, Z. Zhao, Y. Cai, Z. Xu, Y. Yu, Y. Xiong, R. T. K. Kwok, Y. Chen, N. L. C. Leung, D. Ma, J. W. Y. Lam, A. Qin and B. Z. Tang, *Chem. Sci.*, 2018, **9**, 6118.
24. W. Qin, K. Li, G. Feng, M. Li, Z. Yang, B. Liu and B. Z. Tang, *Adv. Funct. Mater.*, 2014, **24**, 635.
25. Y.-C. Lo, T.-H. Yeh, C.-K. Wang, B.-J. Peng, J.-L. Hsieh, C.-C. Lee, S.-W. Liu and K.-T. Wong, *ACS Appl. Mater. Interfaces*, 2019, **11**, 23417.
26. P. Wei, L. Duan, D. Zhang, J. Qiao, L. Wang, R. Wang, G. Dong and Y. Qiu, *J. Mater. Chem.*, 2008, **18**, 806.
27. Y. Huang, Y. Liu, P. J. W. Sommerville, W. Kaminsky, D. S. Ginger and C. K. Luscombe, *Green Chem.*, 2019, **21**, 6600.

28. T. Bura, J. T. Blaskovits and M. Leclerc, *J. Am. Chem. Soc.*, 2016, **138**, 10056.
29. Y. Huang and C. K. Luscombe, *Chem. Rec.*, 2019, **19**, 1039.
30. M. D. McGehee and A. J. Heeger, *Adv. Mater*, 2000, **12**, 1655.
31. Y. Li, X. Zhang, Y. Zhang, R. Dong and C. K. Luscombe, *J. Polym. Sci. A. Polym. Chem.*, 2019, **57**, 201.
32. Z. Yang, Z. Mao, Z. Xie, Y. Zhang, S. Liu, J. Zhao, J. Xu, Z. Chi and M. P. Aldred, *Chem. Soc. Rev.*, 2017, **46**, 915.
33. L. Ying, C.-L. Ho, H. Wu, Y. Cao and W.-Y. Wong, *Adv. Mater.*, 2014, **26**, 2459.
34. Y. Li, J.-Y. Liu, Y.-D. Zhao and Y.-C. Cao, *Mater. Today*, 2017, **20**, 258.
35. X.-H. Zhu, J. Peng, Y. Cao and J. Roncali, *Chem. Soc. Rev.*, 2011, **40**, 3509.
36. T. Liu, L. Zhu, C. Zhong, G. Xie, S. Gong, J. Fang, D. Ma and C. Yang, *Adv. Funct. Mater.*, 2017, **27**, 1606384.
37. Y. Hong, J. W. Y. Lam and B. Z. Tang, *Chem. Soc. Rev.*, 2011, **40**, 5361.
38. C. H. Chen, C. W. Tang, J. Shi and K. P. Klubek, *Macromol. Symp.*, 1998, **125**, 49.
39. T.-H. Liu, C.-Y. Iou and C. H. Chen, *Curr. Appl. Phys.*, 2005, **5**, 218.
40. B. Zhao, T. Zhang, B. Chu, W. Li, Z. Su, H. Wu, X. Yan, F. Jin, Y. Gao and C. Liu, *Sci. Rep.*, 2015, **5**, 10697.
41. L. H. Slooff, N. J. Bakker, P. M. Sommeling, A. Büchtemann, A. Wedel and W. G. J. H. M. van Sark, *Phys. Status Solidi A*, 2014, **211**, 1150.
42. S. Guo, B. Cao, W. Wang, J.-F. Moulin and P. Müller-Buschbaum, *ACS Appl. Mater. Interfaces*, 2015, **7**, 4641.
43. S. B. Schmidt, T. Biskup, X. Jiao, C. R. McNeill and M. Sommer, *J. Mater. Chem. C*, 2019, **7**, 4466.
44. Y. Huang, N. Zheng, Z. W
ang, L. Ying, F. Huang and Y. Cao, *Chem. Comm.*, 2017, **53**, 1997.
45. Y. Huang, W. Xu, C. Zhou, W. Zhong, R. Xie, X. Gong, L. Ying, F. Huang and Y. Cao, *J. Polym. Sci. A. Polym. Chem.*, 2016, **54**, 2119.
46. A. David, P. T. Fini, K. W. Houser, Y. Ohno, M. P. Royer, K. A. G. Smet, M. Wei and L. Whitehead, *Opt. Express*, 2015, **23**, 15888.
47. Y. Peng, H. Wang, J. Liu, Q. Sun, Y. Mou and X. Guo, *ACS Appl. Electron. Mater.*, 2020, **2**, 2929.
48. H. C. Yoon, J. H. Oh, S. Lee, J. B. Park and Y. R. Do, *Sci. Rep.*, 2017, **7**, 2808.
49. A. Shukla, N. R. Wallwork, X. Li, J. Sobus, V. T. N. Mai, S. K. M. McGregor, K. Chen, R. J. Lepage, E. H. Krenske, E. G. Moore, E. B. Namdas and S.-C. Lo, *Adv. Opt. Mater.*, 2020, **8**, 1901350.
50. J. V. Caspar and T. J. Meyer, *J. Phy. Chem.*, 1983, **87**, 952.
51. A. A. Wiles, J. Bruckbauer, N. Mohammed, M. Cariello, J. Cameron, N. J. Findlay, E. Taylor-Shaw, D. J. Wallis, R. W. Martin, P. J. Skabara and G. Cooke, *Mater. Chem. Front.*, 2020, **4**, 1006.
52. N. J. Findlay, J. Bruckbauer, A. R. Inigo, B. Breig, S. Arumugam, D. J. Wallis, R. W. Martin and P. J. Skabara, *Adv. Mater.*, 2014, **26**, 7290.
53. F. Hide, P. Kozodoy, S. P. DenBaars and A. J. Heeger, *Appl. Phys. Lett.*, 1997, **70**, 2664.
54. Z. Li, L. Kong, S. Huang and L. Li, *Angew. Che. In. Ed.*, 2017, **56**, 8134.
55. Y. Kim, S. Ham, H. Jang, J. H. Min, H. Chung, J. Lee, D. Kim and E. Jang, *ACS Appl. Nano Mater.*, 2019, **2**, 1496.
56. H. Guan, S. Zhao, H. Wang, D. Yan, M. Wang and Z. Zang, *Nano Energy*, 2020, **67**, 104279.
57. A. Espasa, M. Lang, C. F. Aguiño, D. Sanchez-deAlcazar, J. P. Fernández-Blázquez, U. Sonnewald, A. L. Cortajarena, P. B. Coto and R. D. Costa, *Nature Communications*, 2020, **11**, 879.
58. V. Fernández-Luna, J. P. Fernández-Blázquez, M. A. Monclús, F. J. Rojo, R. Daza, D. Sanchez-deAlcazar, A. L. Cortajarena and R. D. Costa, *Mater. Horiz.*, 2020, **7**, 1790.
59. L. Niklaus, S. Tansaz, H. Dakhil, K. T. Weber, M. Pröschel, M. Lang, M. Kostrzewa, P. B. Coto, R. Detsch, U. Sonnewald, A. Wierschem, A. R. Boccaccini and R. D. Costa, *Adv. Funct. Mater.*, 2017, **27**, 1601792.
60. W. H. Kim, Y. J. Jang, J.-Y. Kim, M. Han, M. Kang, K. Yang, J.-H. Ryou and M.-K. Kwon, *Appl. Sci.*, 2020, 2112.
61. M. Xi, F. Jean Paul, N. Nadarajah and D. B. John, *J. Biomed. Opt.*, 2017, **22**, 055004.